



**HAL**  
open science

## Transient melt formation and its effect on conversion phenomena during nuclear waste vitrification – HT-ESEM analysis

Richard Pokorný, Miroslava Vernerová, Jaroslav Kloužek, Petra Cincibusová, Martina Kohoutková, Radek Pezl, Pavel Ferkl, Pavel Hrma, Renaud Podor, Sophie Schuller, et al.

### ► To cite this version:

Richard Pokorný, Miroslava Vernerová, Jaroslav Kloužek, Petra Cincibusová, Martina Kohoutková, et al.. Transient melt formation and its effect on conversion phenomena during nuclear waste vitrification – HT-ESEM analysis. *Journal of the American Ceramic Society*, 2023, 107 (3), pp.1691-1705. 10.1111/jace.19361 . hal-04487934

**HAL Id: hal-04487934**

**<https://hal.univ-lille.fr/hal-04487934>**

Submitted on 20 Mar 2024

**HAL** is a multi-disciplinary open access archive for the deposit and dissemination of scientific research documents, whether they are published or not. The documents may come from teaching and research institutions in France or abroad, or from public or private research centers.





L'archive ouverte pluridisciplinaire **HAL**, est destinée au dépôt et à la diffusion de documents scientifiques de niveau recherche, publiés ou non, émanant des établissements d'enseignement et de recherche français ou étrangers, des laboratoires publics ou privés.



Distributed under a Creative Commons Attribution 4.0 International License

## SPECIAL ISSUE ARTICLE

# Transient melt formation and its effect on conversion phenomena during nuclear waste vitrification – HT-ESEM analysis

Richard Pokorný<sup>1,2</sup>  | Miroslava Vernerová<sup>1,2</sup> | Jaroslav Kloužek<sup>1,2</sup> |  
 Petra Cincibusová<sup>1,2</sup>  | Martina Kohoutková<sup>1</sup> | Radek Pezl<sup>1</sup> | Pavel Ferkl<sup>3</sup>  |  
 Pavel Hрма<sup>4</sup> | Renaud Podor<sup>5</sup>  | Sophie Schuller<sup>6</sup> | Albert A. Kruger<sup>7</sup>

<sup>1</sup>University of Chemistry and Technology  
Prague, Prague, Czech Republic

<sup>2</sup>Institute of Rock Structure and  
Mechanics of the Czech Academy of  
Sciences, Prague, Czech Republic

<sup>3</sup>Pacific Northwest National Laboratory,  
Richland, Washington, USA

<sup>4</sup>AttainX, Support Services Contractor to  
the Office of River Protection, U.S.  
Department of Energy, Richland,  
Washington, USA

<sup>5</sup>ICSM, CNRS, ENSCM, CEA, Univ  
Montpellier, Marcoule, France

<sup>6</sup>CEA, DES, ISEC, DPME, Université  
Montpellier, Bagnols-sur-Cèze, France

<sup>7</sup>U.S. Department of Energy, Office of  
River Protection, Richland, Washington,  
USA

## Correspondence

Richard Pokorný, Technicka 5/1905, 166  
28, University of Chemistry and  
Technology Prague, Prague 6, Czechia.  
Email: Richard.Pokorny@vscht.cz

## Funding information

Czech Ministry of Education, Youth and  
Sports, Grant/Award Number:  
LUAUS23062; U.S. Department of Energy  
(DOE) Waste Treatment and  
Immobilization Plant Project

## Abstract

Although the vitrification of nuclear waste has a decades-long history, numerous opportunities still exist to improve its efficiency and to increase the waste loading in glass. This is especially true for the vitrification of low-activity waste (LAW), which has been historically treated by other immobilization technologies and is less mature than high-level waste (HLW) vitrification. In this work, we address one of the least understood phenomena during the conversion of nuclear waste feeds to glass—the formation of molten salt and transient glass-forming melt. Using high-temperature environmental scanning electron microscopy (HT-ESEM) in combination with X-ray diffraction, thermogravimetry, and evolved gas analysis, we have analyzed the complex chemical reactions and phase transitions as they occur during melting of representative HLW and LAW melter feeds. We evaluated the compositions of amorphous phases and the fractions of salt components, and estimated the fractions of molten salt phases present in the feeds as a function of temperature. We show that the maximum fraction of molten salts is ~4 % and ~28 % during HLW and LAW feed melting, respectively, and discuss the possibility of molten salt migration in LAW feeds. We also argue that the presence of significant fractions of molten salt phase can hinder the retention of rhenium (and, hence, radioactive technetium), and discuss how the properties of molten salt phase and transient glass-forming melt are related to primary foam formation and behavior. Finally, we summarize key unanswered questions requiring further research to increase the understanding of the conversion process and enhance the nuclear waste vitrification efficiency.

## KEYWORDS

glass melting, molten salt, nuclear waste, scanning electron microscopy, segregation, volatilization

This is an open access article under the terms of the [Creative Commons Attribution](https://creativecommons.org/licenses/by/4.0/) License, which permits use, distribution and reproduction in any medium, provided the original work is properly cited.

© 2023 The Authors. *Journal of the American Ceramic Society* published by Wiley Periodicals LLC on behalf of American Ceramic Society.

## 1 | INTRODUCTION

The Hanford Site, located in Washington State, USA, is one of the most contaminated nuclear sites in the world, with approximately 56 million gallons of radioactive waste historically stored in 177 underground tanks.<sup>1,2</sup> The waste contains a complex mixture of radionuclides, heavy metals, and other hazardous compounds, making it difficult to manage and dispose of safely. To address this issue, the U.S. Department of Energy plans to vitrify the waste—both high-level waste (HLW) and low-activity waste (LAW) fractions—using all-electric melters. The vitrification process involves combining the waste with glass-forming materials, such as silica and boric acid, and heating it to 1150°C to produce a highly durable solid glass matrix that can safely contain the radioactive and hazardous waste over long periods of time.<sup>3–6</sup>

During the vitrification process, a layer of reacting and melting material, known as the cold cap, forms on top of the molten glass.<sup>5,7,8</sup> In the cold cap, various complex physical and chemical processes occur, including water evaporation, melting of oxyanionic salts, borate melt formation, reactions between the borate melt, molten salts, and solids, precipitation of intermediate crystalline phases, primary foam formation, growth, and collapse, and the dissolution of residual refractory particles.<sup>9–12</sup> These processes proceed over a wide range of time- and length-scales—from the reaction kinetics on the molecular-scale, to silica dissolution and glass-forming melt formation on the micro-scale, to foam expansion and collapse on the macro-scale. An improved understanding of these physico-chemical processes occurring in the cold cap is critical for optimizing the vitrification process, including achieving a consistent high melting rate,<sup>13,14</sup> maximizing the retention of volatile elements (e.g., technetium or iodine),<sup>15,16</sup> and limiting the formation of crystalline species (e.g., nepheline) that can compromise the quality of the final product.<sup>17,18</sup> This is especially true for the vitrification of low-activity waste, which is a technologically much less mature process, because LAW was historically treated using other technologies, such as cementation, bituminization, or compaction and containerization.<sup>19–21</sup>

Over the past decade, our understanding of the melting process was significantly improved by measuring and analyzing a vast volume of data on feed responses to heating in terms of chemical reactions and phase transitions that occur as temperature increases.<sup>7,22–31</sup> Despite this significant research effort, open questions still intrigue us, such as the coexistence of molten oxyanionic salts and the glass-forming borate melt in the early stages of conversion, or the relationship between the glass-forming melt fraction and the properties and characteristics of primary foaming.

These knowledge gaps highlight the need for new experimental techniques that can provide additional insights into the melting process.

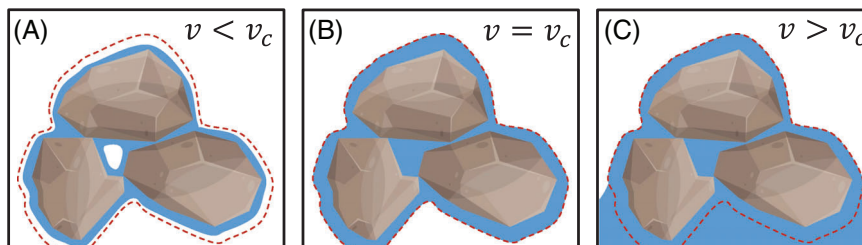
In this paper, we used high-temperature environmental scanning electron microscopy (HT-ESEM) to obtain direct experimental evidence about the morphology evolution during the melting of nuclear waste feeds.<sup>32–34</sup> Thus far, such morphological analysis was limited to high-temperature in situ visual and X-ray observation methods,<sup>26,29</sup> each with their own advantages and drawbacks, or to *ex-situ* analysis of samples quenched to room temperature.<sup>28</sup> HT-ESEM allows us to directly observe, as a function of temperature, the microstructure and phase evolutions, including the formation of low-temperature liquids (eutectic salt melt and glass-forming borate melt), intermediate crystal phases, and the onset of foaming. By combining HT-ESEM with other experimental techniques, such as X-ray diffraction (XRD), evolved gas analysis (EGA), thermogravimetric analysis (TGA), or leaching tests, we were able to estimate the fraction of liquid phases during the melting of two representative HLW and LAW nuclear waste feeds, and use this information to discuss the potential for molten salt migration—a demixing phenomenon that can occur during feed melting in the cold cap and potentially compromise the formation of a steady-state melting process.<sup>35</sup> We also address the relationship between molten salts, glass-forming melt, and retention of rhenium, a nonradioactive surrogate for technetium, showing that the high fractions of molten salt that evolve during LAW melting can negatively affect the Tc/Re retention.

Finally, we discuss the effect of the transient glass-forming melt properties, such as the viscosity and the presence of undissolved crystalline phases, on the characteristics of the primary foam, such as the foam onset and foam collapse temperatures, and foam porosity.<sup>36</sup> By understanding the relationship between the glass-forming melt composition, properties, and primary foaming, our ultimate goal is to develop feed formulation strategies leading to primary foam minimization to achieve a more stable and efficient nuclear waste vitrification process.

## 2 | MOLTEN SALT MIGRATION

During the melting of a feed in a cold cap, the condensed phase consists of various liquid and solid phases. The molten salt phase, also called primary melt, which consists of various oxyanionic salts (mainly carbonates, nitrates, nitrites, borates, sulfates, and chromates) and is as fluid as water, and therefore, highly mobile, wets surfaces of solids and the nascent glass-forming melt, reacting with them

**FIGURE 1** Schematic illustration of refractory melting in feeds with different fraction of molten salts (A) low fractions of molten salt,  $v < v_c$ , (B) at critical salt volume fraction  $v = v_c$  (denoted by red dashed line), and (C) gravitational salt migration when  $v > v_c$ .



while releasing ample volumes of gases, mainly CO<sub>2</sub>, NO, and O<sub>2</sub>.

While the presence of primary melt is desirable, as it accelerates the conversion process, its excessive fraction can lead to an unwanted phenomenon of molten salt migration (demixing and drainage) that can occur when the melt fraction is higher than that which can be immobilized by capillary forces in liquid films and bridges between the solid particles.<sup>35</sup> Whereas vertical drainage is harmless, horizontal migration can potentially disrupt long-term steady-state melting by leaving behind slowly melting refractory material. A general condition for gravitationally driven salt migration in a bed of granular solids is expressed by the inequality<sup>35</sup>

$$v_c < v < 1 - v_s \quad (1)$$

where  $v$  is the molten salt volume fraction, and  $v_c$  and  $v_s$  denote the critical primary melt volume fraction and the solid volume fraction, respectively. The value of  $v_c$  corresponds to the melt volume needed for coating and bridging of the solid particles and depends on the specific surface area of the particles, the melt viscosity, and the melt-solid interfacial tension; when  $v < v_c$ , no drainage occurs (Figure 1A). If  $v$  exceeds  $v_c$ , capillary forces no longer immobilize primary melt on the surface of the solid particles, and the excess volume ( $v - v_c$ ) can drain (Figure 1C). In a rather hypothetical situation when  $v > 1 - v_s$ , the volume of molten salts is higher than the space available between grains, and the grains can either settle or float in the connected liquid, according to the difference between their density and the density of the salt melt.

Hrma et al.<sup>35</sup> studied the gravitational drainage of a primary melt in a glass batch consisting of Na<sub>2</sub>CO<sub>3</sub>, Li<sub>2</sub>CO<sub>3</sub>, (both alkali carbonates crushed to < 75 μm), and SiO<sub>2</sub> (0.1–0.4 mm crushed quartz particles) at 600°C, at which the primary melt did not yet react with silica particles. The onset of gravity-driven drainage occurred when more than half of the intergranular space was filled with the salt melt. Since, in their study, the fraction of intergranular space was  $1 - v_s = 0.43$ , drainage was avoided when  $v < 0.22$ . In another study, Kim et al.<sup>37</sup> reported that the drainage occurred when  $v > \sim 0.3$ .

## 3 | EXPERIMENTAL

### 3.1 | Feed preparation

Tables 1 and 2 list the compositions of simulant HLW and LAW melter feeds and glasses used in this study, formulated by the Vitreous State Laboratory of the Catholic University of America.<sup>38</sup> The HLW feed (called “Al-19”) is based on a high alumina high-level waste composition. The LAW feed (called “AP-107”) is based on the supernatant composition in Hanford tank 241-AP-107.<sup>39</sup> For both HLW and LAW, slurry feeds were prepared by adding the chemicals and minerals, listed in Table 1, to deionized water while stirring.<sup>40</sup> The slurries were dried, first on a 90°C hot-plate and then overnight in an oven at 109°C. The dried feeds were crushed and milled to powder in a planetary ball mill (Fritsch Pulverisette 6, 10 grinding balls 20 mm diameter, 10 min at 300 rpm) to under 100 μm grain size.

### 3.2 | Feed characterization

The feed conversion to glass was characterized using in-situ environmental scanning electron microscopy at high temperature (HT-ESEM), X-ray diffraction (XRD), evolved gas analysis (EGA), thermogravimetric analysis (TGA), and feed expansion test (FET).

A 5-mm diameter platinum crucible with a few milligrams of powdered feed was placed in the HT-ESEM (Quanta 200 ESEM FEG by FEI Company) high-temperature furnace (heating stage 1400, FEI) equipped with a second thermocouple that allowed a precise temperature measurement<sup>32</sup> during the ramp heating to 1000°C at 5 K min<sup>-1</sup>. The ESEM was operated at 12 kV with a beam current close to 0.5 nA, in order to avoid any beam effect on the samples during the experiments. A gaseous secondary electron detector was used to record SE images of sample surface. The air pressure in the ESEM chamber was ranging between 100–150 Pa during the experiments. Sample images were continuously recorded at a fixed location during heating. To detect the undissolved crystalline solid phases, ~4 g feed samples were heated in porcelain crucibles at 10 K min<sup>-1</sup> to temperatures from 200°C

**TABLE 1** Melter feed compositions—Waste simulant and glass-forming and -modifying additives (GFMA)—In g to make 1 kg of high-level waste (HLW) (Al-19) and low-activity waste (LAW) (AP-107) glass.

| Melter feed component   | HLW      | LAW      |
|---|----------|----------|
| Waste simulant  | Mass (g) | Mass (g) |
| Al(NO <sub>3</sub> ) <sub>3</sub> •9H <sub>2</sub> O            |          | 134.13   |
| Al(OH) <sub>3</sub>   | 369.0    |          |
| Ca(NO <sub>3</sub> ) <sub>2</sub> •4H <sub>2</sub> O            |          | 0.30     |
| Bi <sub>2</sub> O <sub>3</sub>                                  | 11.6     |          |
| CaO   | 11.0     |          |
| Fe(NO <sub>3</sub> ) <sub>3</sub> •9H <sub>2</sub> O            |          | 0.18     |
| NiO   |          | 0.04     |
| Cr <sub>2</sub> O <sub>3</sub> •1.5H <sub>2</sub> O             | 6.2      |          |
| Na <sub>2</sub> CrO <sub>4</sub> •4H <sub>2</sub> O             |          | 2.28     |
| Fe(OH) <sub>3</sub>   | 63.2     |          |
| FePO <sub>4</sub> •2H <sub>2</sub> O                            | 27.9     |          |
| KNO <sub>3</sub>  | 3.0      |          |
| KOH   |          | 5.25     |
| MgO   | 1.2      |          |
| NaOH  | 20.4     | 84.61    |
| Ni(OH) <sub>2</sub>   | 5.0      |          |
| PbO   | 4.1      | 0.02     |
| NaCl  |          | 6.68     |
| NaF   | 14.9     | 0.89     |
| Na <sub>3</sub> PO <sub>4</sub> •12H <sub>2</sub> O             |          | 6.80     |
| Na <sub>2</sub> SO <sub>4</sub>                                 | 3.6      | 7.68     |
| NaNO <sub>2</sub>   | 3.5      | 75.32    |
| NaNO <sub>3</sub>   | 12.4     | 68.59    |
| Na <sub>2</sub> CO <sub>3</sub>                                 |          | 55.97    |
| ZnO   | 0.8      |          |
| Zr(OH) <sub>4</sub> •xH <sub>2</sub> O (x = 0.654)              | 5.5      |          |
| NaC <sub>2</sub> H <sub>3</sub> O <sub>2</sub>                  |          | 3.35     |
| NaCHO <sub>2</sub>  |          | 3.65     |
| Na <sub>2</sub> C <sub>2</sub> O <sub>4</sub>                   |          | 0.94     |
| H <sub>2</sub> C <sub>2</sub> O <sub>4</sub> •2H <sub>2</sub> O | 1.2      |          |
| Glass-formers and -modifiers                                    | Mass (g) | Mass (g) |
| Al <sub>2</sub> SiO <sub>5</sub>                                |          | 69.49    |
| H <sub>3</sub> BO <sub>3</sub>                                  | 342.6    | 177.05   |
| CaSiO <sub>3</sub>  | 97.1     | 82.57    |
| Fe <sub>2</sub> O <sub>3</sub>                                  |          | 55.07    |
| Li <sub>2</sub> CO <sub>3</sub>                                 | 89.2     | 21.87    |
| Mg <sub>2</sub> SiO <sub>4</sub>                                |          | 28.30    |
| Na <sub>2</sub> CO <sub>3</sub>                                 | 106.6    |          |
| SiO <sub>2</sub>  | 221.1    | 360.90   |
| TiO <sub>2</sub>  |          | 14.55    |
| ZnO   |          | 35.06    |
| ZrSiO <sub>4</sub>  |          | 44.67    |
| C <sub>12</sub> H <sub>22</sub> O <sub>11</sub>                 |          | 58.55    |
| Total   | 1421.9   | 1404.75  |

**TABLE 2** High-level waste (HLW) (Al-19) and low-activity waste (LAW) (AP-107) glass compositions in mass %.

| Glass                          | HLW   | LAW   |
|--------------------------------|-------|-------|
| Al <sub>2</sub> O <sub>3</sub> | 23.97 | 6.19  |
| B <sub>2</sub> O <sub>3</sub>  | 19.19 | 9.97  |
| Bi <sub>2</sub> O <sub>3</sub> | 1.14  |       |
| CaO                            | 5.58  | 3.99  |
| Cl                             |       | 0.40  |
| Cr <sub>2</sub> O <sub>3</sub> | 0.52  | 0.10  |
| F                              | 0.67  | 0.04  |
| Fe <sub>2</sub> O <sub>3</sub> | 5.90  | 5.49  |
| K <sub>2</sub> O               | 0.14  | 0.44  |
| Li <sub>2</sub> O              | 3.57  | 0.88  |
| MgO                            | 0.12  | 1.61  |
| Na <sub>2</sub> O              | 9.58  | 16.95 |
| NiO                            | 0.40  | 0.004 |
| P <sub>2</sub> O <sub>5</sub>  | 1.05  | 0.25  |
| PbO                            | 0.41  | 0.002 |
| SO <sub>3</sub>                | 0.20  | 0.43  |
| SiO <sub>2</sub>               | 27.00 | 45.40 |
| TiO <sub>2</sub>               |       | 1.45  |
| ZnO                            | 0.08  | 3.49  |
| ZrO <sub>2</sub>               | 0.39  | 2.99  |
| SUM                            | 100   | 100   |

to 1100°C in 100°C increments and quenched in air. The samples were then milled and analyzed using an XRD diffractometer (PANalytical X'Pert<sup>3</sup> Powder) using continuous scan type, 5 to 80° 2θ angular range, 0.04° step size, 115 s scan step, Cu Kα anode, 40 kV, 30 mA generator settings, with PIXcel1D detector (Malvern). Rietveld refinement was carried out using Highscore Plus software and amorphous fractions were obtained using the external standard method with SiO<sub>2</sub>-quartz as the standard. To evaluate the individual and overall gas evolution, ~1 g feed samples loaded in quartz crucibles were analyzed using EGA (gas chromatograph Agilent 6890 N with a mass spectrometric detector Agilent 5973 N) and ~30 mg samples loaded in platinum crucibles were analyzed using TGA (Setaram Setsys). During both EGA and TGA, feeds were heated at 10 K min<sup>-1</sup> from room temperature to 1150°C under He atmosphere. Finally, the feed volume and porosity were evaluated as a function of temperature using FET: a uniaxially pressed ~1 g feed pellet, 13 mm in diameter, was heated from room temperature to 1150°C at 10 K min<sup>-1</sup> in a high-temperature observation furnace and its volume was evaluated from the sample profile area. The XRD, EGA, TGA, and FET experimental procedures are described in full detail in our previous study.<sup>28</sup>

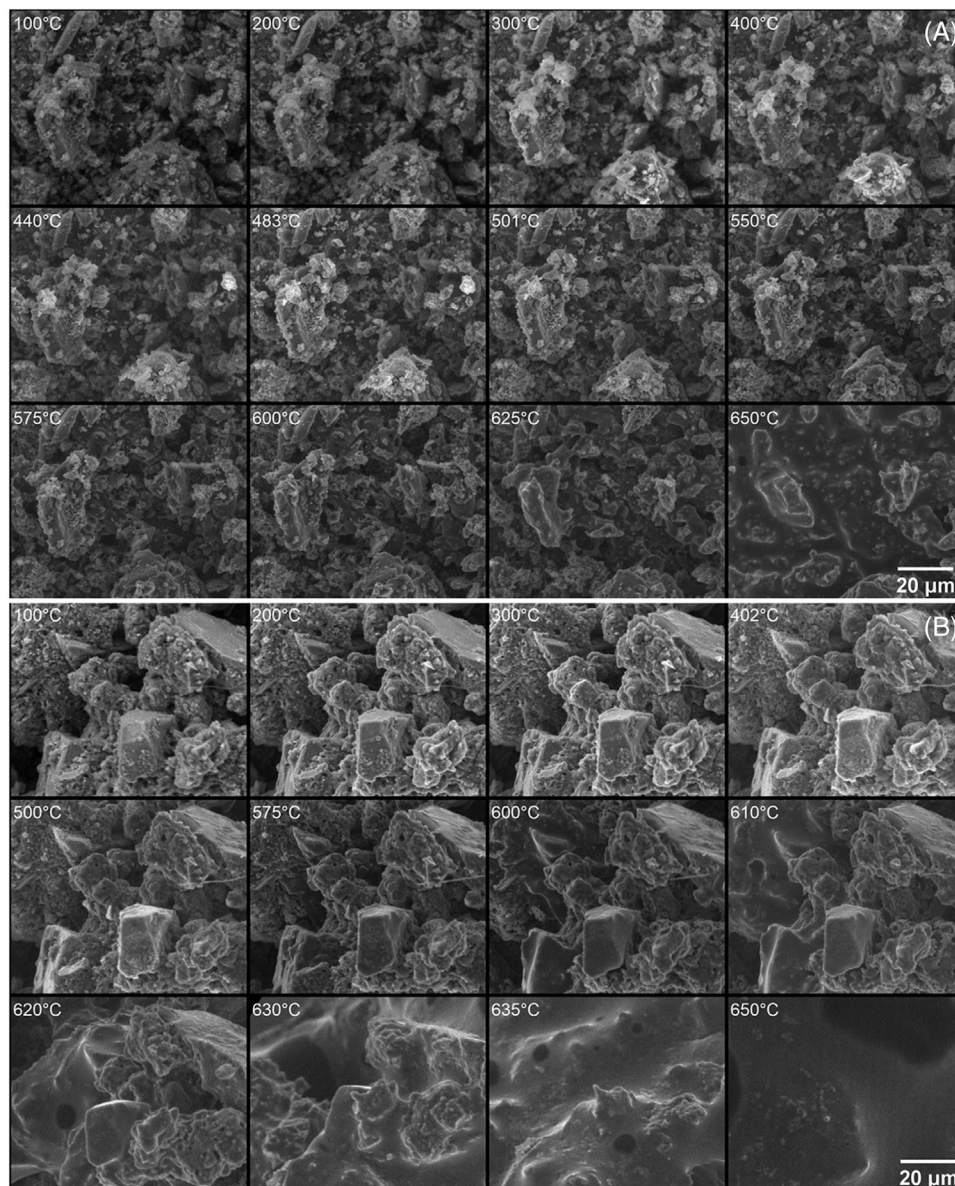


**FIGURE 2** Snapshots of the high-temperature environmental scanning electron microscopy (HT-ESEM) movies showing the morphology evolution in (A) high-level waste (HLW) and (B) low-activity waste (LAW) melter feeds. Full movies showing the solid-liquid transformations are provided in supplementary files.

## 4 | RESULTS

Figure 2 displays a series of HT-ESEM images taken during the melting of HLW and LAW feed samples (full videos are available as [Supplementary Files](#)). Figure 3 displays the corresponding crystalline phase compositions evaluated by ex-situ XRD (the diffraction patterns are provided in the Supplement, Figure S1). Figure 4 overlays the normalized feed volume, measured by FET, with the individual gas evolution rate measured by EGA and overall mass loss rate measured by TGA. The grey area in Figures 3 and 4 indicate the temperature range of primary foaming in the cold cap, that is, the temperature region

between the onset of foaming (corresponding to the local minima of the feed porosity in Figure 4) and the cold cap foam bottom temperature, defined as a temperature at which vigorous primary gas evolution stops and the foam collapses.<sup>13</sup> The secondary HLW peak corresponds to secondary foaming—note that while primary and secondary foaming are geometrically separated under the cold cap (secondary foaming occurs within the melt below the cold cap), they can overlap during FET measurements.<sup>36</sup>

Feed components start reacting already during slurry preparation and drying. As previously reported by Xu et al.<sup>22,23</sup> and Hujova et al.,<sup>41</sup> boric acid and sodium hydroxide create an amorphous sodium-borate phase. Because

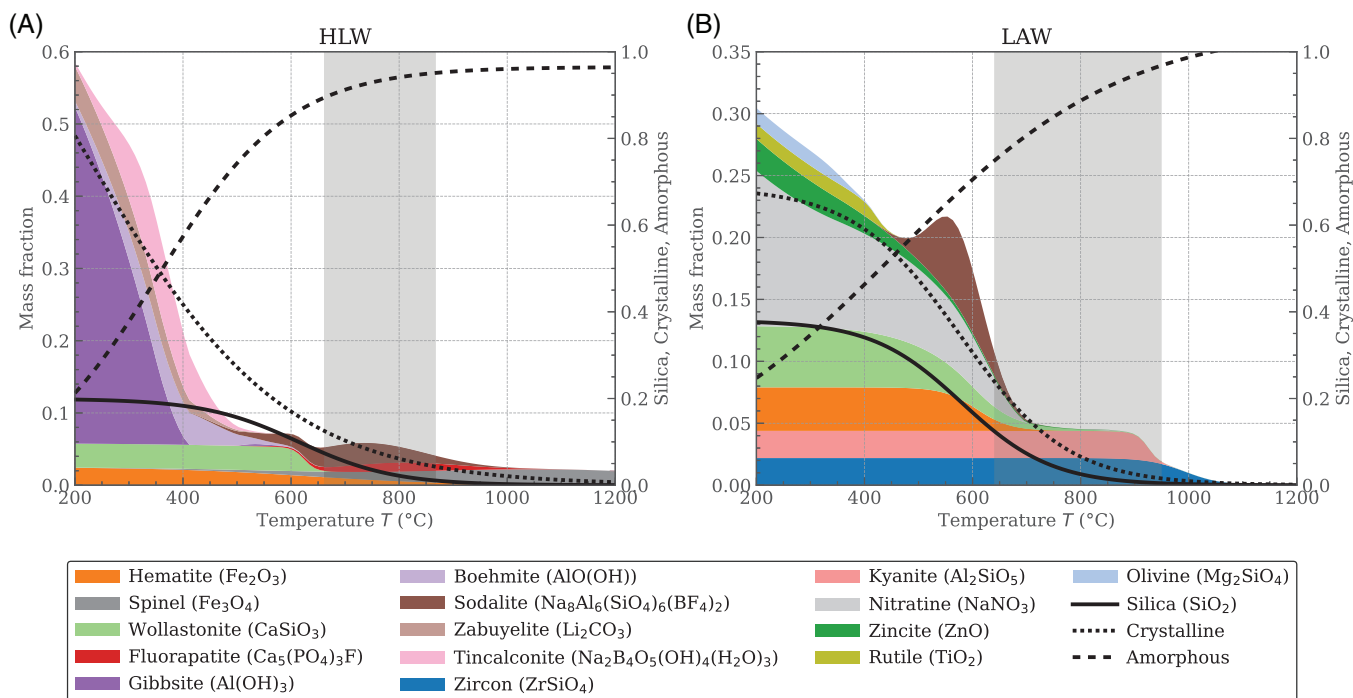


**FIGURE 3** Crystalline phase evolution (smoothed by sigmoidal or Gaussian functions) in (A) high-level waste (HLW) and (B) low-activity waste (LAW) feeds heated at  $10 \text{ K min}^{-1}$ . The gray area indicates the primary foaming range. Data for HLW melter feed Al-19 adapted from Ferkl et al.<sup>28</sup> with permission from Elsevier.

there are no alkali-borate crystals (such as borax) visible on XRD, and because the slurry feed contains a large amount of free water, our current hypothesis is that this sodium-borate phase has a gel structure. However, we did not attempt to experimentally confirm this; it is also theoretically possible that it can already be a glassy phase, but we do not expect it at these low temperatures. The sodium-borate phase, on heating, reacts with oxyanionic components and dissolves oxide components while turning into the nascent glass-forming melt. As described by Xu et al.,<sup>23</sup> reactions with carbonates, nitrates, and nitrites enrich the borate phase with alkali and alkaline earth oxides while evolving gases. Simultaneously, the borate phase dissolves amorphous  $\text{Al}_2\text{O}_3$  and  $\text{Fe}_2\text{O}_3$  from hydroxides as well as minor components, such as  $\text{NiO}$ ,  $\text{ZnO}$ , or  $\text{PbO}$ , and eventually  $\text{ZrO}_2$  and  $\text{SiO}_2$ . Figure 5 presents the composition of the amorphous phase, in terms of mass fractions of major components, estimated based on the batch compositions and the chemical compositions of crystalline phases identified with XRD.

The oxyanionic salt fraction (carbonates, nitrates, nitrites, sulfates, chromates, borates, halides, alkali hydroxides, and organics) is as high as 42 % in the HLW feed, and 50 % in the LAW feed (see Figure 6). Initially consisting of a mixture of crystalline compounds, it forms multicomponent eutectic melts during heating, creating a

low-viscosity liquid phase that wets the borate gel phase and the solid components.

According to TGA and EGA, the oxyanionic salt fraction (solids and primary melt) gradually decreases as temperature increases: hydroxides lose  $\text{H}_2\text{O}$  between 100 and  $400^\circ\text{C}$ , carbonates lose  $\text{CO}_2$  between 300 and  $600^\circ\text{C}$  and nitrates with nitrites lose  $\text{NO} + \text{O}_2$  between 400 and  $700^\circ\text{C}$  (or between  $200\text{--}700^\circ\text{C}$  in LAW feeds, where significant amounts of organics are present that react with nitrates and nitrites<sup>42</sup>), losing their cations to the borate melt. Sulfates, halides, and chromates do not decompose, and eventually dissolve in the glass-forming melt, from which  $\text{SO}_2 + \text{O}_2$  may evolve at high temperatures in the form of secondary bubbles. “Others” in Figure 6 represent residual salts and organics— $\text{Na}_2\text{C}_2\text{O}_4$ ,  $\text{Na}_2\text{SO}_4$ , and  $\text{NaNO}_2$  for HLW, and  $\text{Ca}(\text{NO}_3)_2 \cdot 4\text{H}_2\text{O}$ ,  $\text{Fe}(\text{NO}_3)_3 \cdot 9\text{H}_2\text{O}$ ,  $\text{KOH}$ ,  $\text{Na}_2\text{CrO}_4 \cdot 4\text{H}_2\text{O}$ ,  $\text{NaCl}$ ,  $\text{NaF}$ ,  $\text{Na}_2\text{SO}_4$ ,  $\text{NaC}_2\text{H}_3\text{O}_2$ ,  $\text{NaCHO}_2$ , and  $\text{Na}_2\text{C}_2\text{O}_4$  for LAW. The fractions of the sodium borate phase in the oxyanionic salt mixture displayed in Figure 6 were estimated based on leaching tests performed by Xu et al.<sup>22</sup> and Jin et al.<sup>43</sup>

During HT-ESEM, the formation of primary melt is visible as initially sharp edges of the feed particles are rounded and tiny pores are being filled—in LAW feed, this occurs when sucrose melts at  $180^\circ\text{C}$  and starts reacting with nitrates and nitrites (Figure 7B shows traces

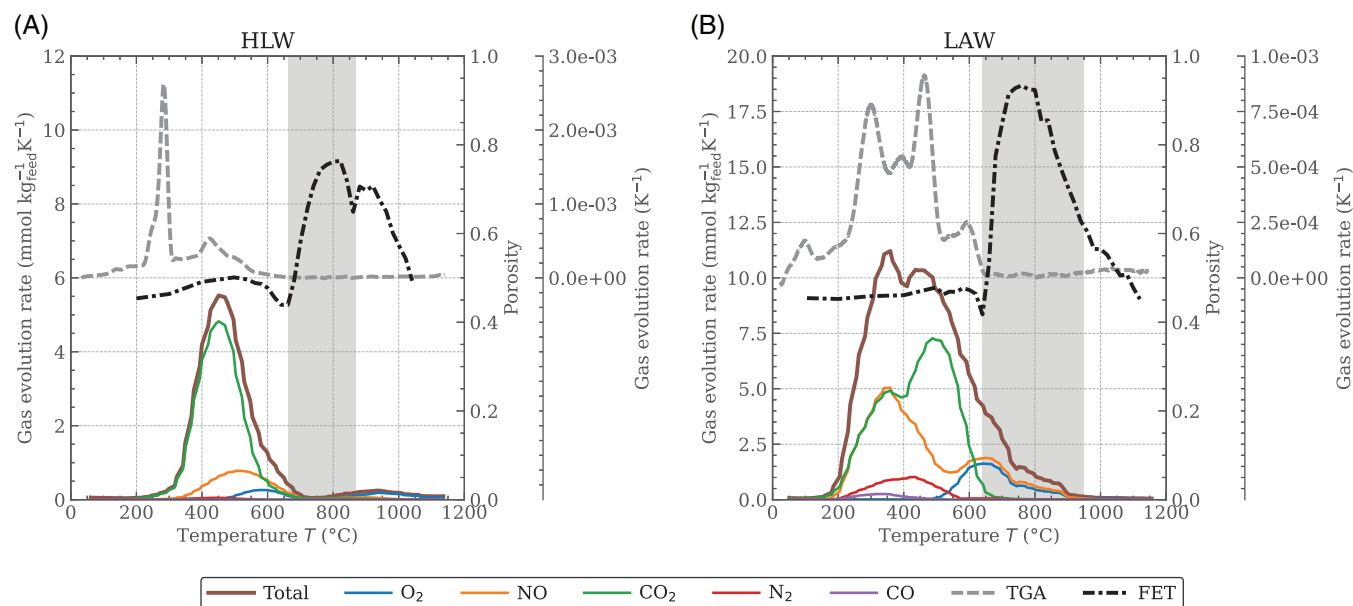


**FIGURE 4** Gas evolution rate based on evolved gas analysis (EGA) (colored solid lines) and thermogravimetric analysis (TGA) (black dashed line) and porosity based on feed expansion test (FET) (black dash-dotted line) during (A) high-level waste (HLW) and (B) low-activity waste (LAW) feed sample heating at  $10 \text{ K min}^{-1}$ . The gray area indicates the primary foaming range.

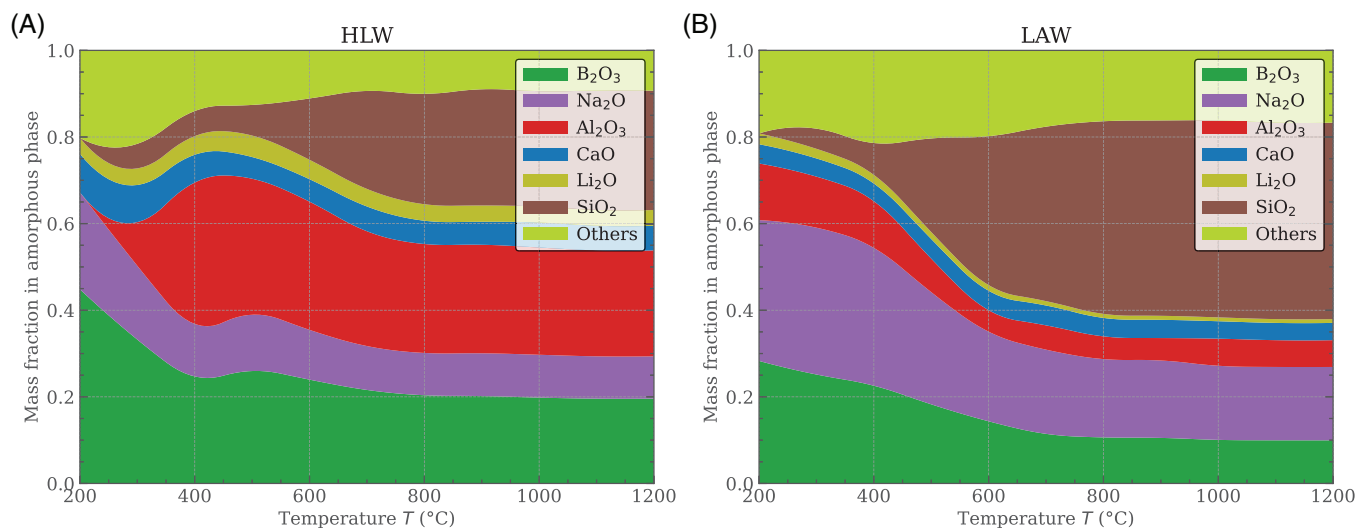


**FIGURE 5** Composition of amorphous phase versus temperature during melting of (A) high-level waste (HLW) and (B) low-activity waste (LAW) melter feed, estimated based on the feed composition and crystalline phase composition obtained by X-ray diffraction (XRD).

of primary melt in the feed at  $256^\circ\text{C}$ ). These reactions produce ample amounts of  $\text{NO}$ ,  $\text{CO}_2$ ,  $\text{H}_2\text{O}$ , and  $\text{N}_2$ , and peak around  $300^\circ\text{C}$ . As the temperature increases above  $300^\circ\text{C}$ , a significant fraction of salt melt visibly evolves in the LAW feed, covering the surface of solid particles (Figure 7C). Upon further heating above  $400^\circ\text{C}$ , a significant fraction of primary melt is gone, leaving behind tiny sub-micron-sized particles dispersed on the larger particle surfaces (Figure 7D), likely a nitrite-sodalite

phase,  $\text{Na}_8(\text{AlSiO}_4)_6(\text{NO}_2)_2$ , which redissolves in the glass melt by  $600^\circ\text{C}$  (Figure 7F). Silica starts to slowly dissolve in the borate phase at  $450^\circ\text{C}$ ; its dissolution rate peaks between  $600\text{--}700^\circ\text{C}$  after the glass-forming melt is completely connected (Figure 7F), trapping gases into primary foam, while silica and alumino-silicate phases continue to dissolve. Few solids remain above  $900^\circ\text{C}$ , as the foam collapses and forms bubble-free molten glass.



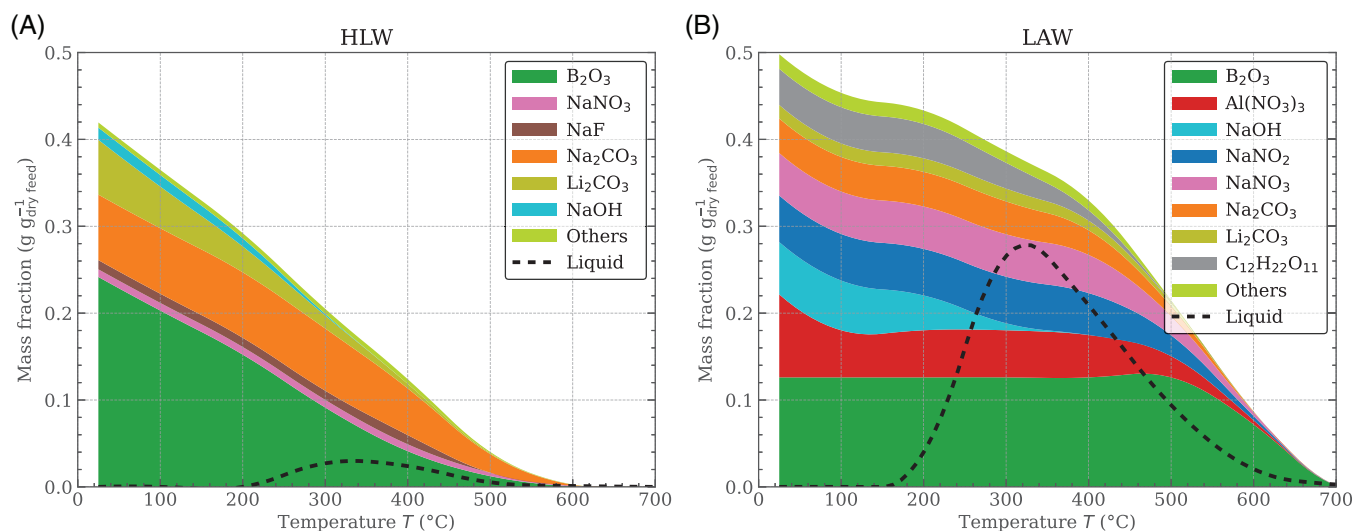


**FIGURE 6** Fraction of salt components with respect to (A) high-level waste (HLW) and (B) low-activity waste (LAW) dry feeds. The black dashed line represents the fraction of liquid molten salt phase estimated in Section 5.1.

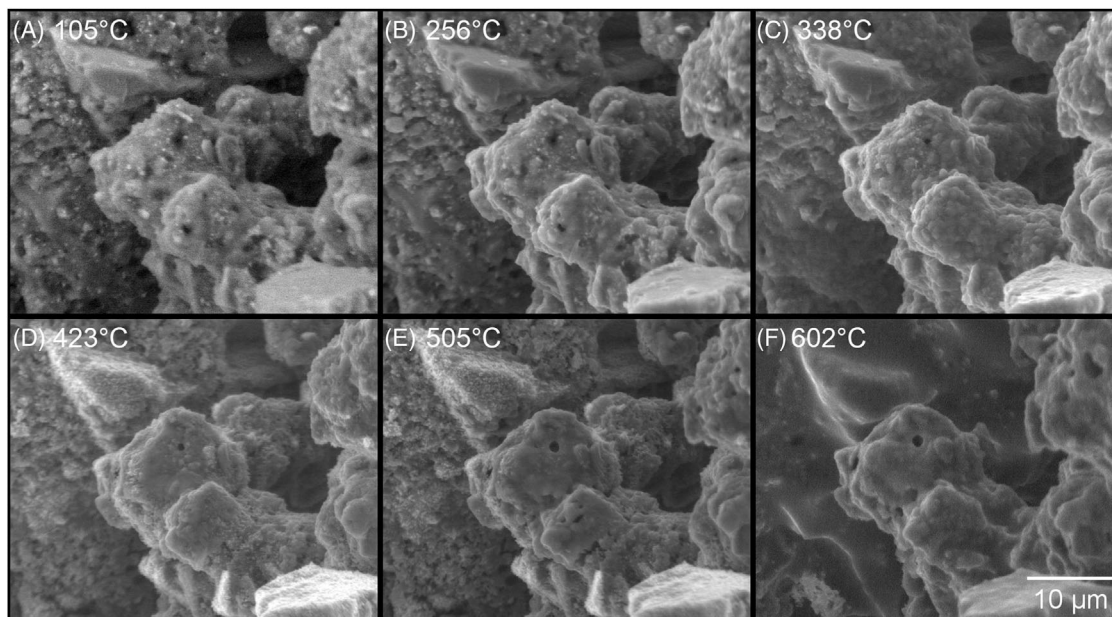


**FIGURE 7** Morphology evolution in low-activity waste (LAW) melter feeds measured by high-temperature environmental scanning electron microscopy (HT-ESEM), showing the formation of primary melt and transient glass-forming melt. (A) Dried LAW feed; (B) first melt starts to appear, consisting of molten sucrose and early eutectics, rounding the particle edges, (C) particles are covered by molten salt phase, (D) liquid phase fraction is visibly decreased as a result of reactions between organics and nitrates/nitrites, producing sub-micron particles (likely a nitrite-sodalite), (E) and (F) borates and silicates start to react and dissolve, producing glass-forming melt.

## 5 | DISCUSSION

### 5.1 | Fraction of molten salts

The formation of the molten salt mixture remains one of the least understood phenomena during waste glass melting. The low-temperature eutectics are important for the

understanding of the actual melting process, accelerating the reactions between organics and nitrates and the reactions between fluxes and refractory components. While the oxyanionic salt fraction of melter feed is as high as 42 % in the HLW feed, and 50 % in the LAW feed (see Figure 6), the liquid primary melt fraction is relatively low, as some feed components react early, a significant fraction

of alkali borates persist in the form of gel, and some crystals of oxyanionic salts dissolve only gradually in the primary melt.

While binary, ternary, or even quaternary phase diagrams exist to estimate the phase composition of simple mixtures (for example, NaOH and KOH, with melting temperatures  $T_m = 323^\circ\text{C}$  and  $360^\circ\text{C}$ , respectively, form mixture with eutectic temperature as low as  $167^\circ\text{C}$ ), the large number and diversity of salts present in the nuclear waste feeds leave us without a proper tool to evaluate the phase composition. For example, the melting point of  $\text{Na}_2\text{CO}_3$ , a common waste component in the LAW feeds and one of the main HLW feed additives, is  $858^\circ\text{C}$ , but the eutectic mixtures of  $\text{Na}_2\text{CO}_3$  with other feed components have melting points as low as  $510^\circ\text{C}$  (with  $\text{Li}_2\text{CO}_3$ ) and as low as  $283^\circ\text{C}$  (with NaOH). In addition,  $\text{Na}_2\text{CO}_3$  starts to react with  $\text{SiO}_2$  at temperatures as low as  $550^\circ\text{C}$ . Thus, the amount of  $\text{Na}_2\text{CO}_3$  dissolved in the primary melt is highly dependent on its fraction in the feed and on the primary melt composition.

The primary melt fraction, shown in Figure 6, was thus estimated using the following assumptions:

- At  $100^\circ\text{C}$ , no molten salt is present. While some of the feed hydrates have lower melting points, they are dehydrated and/or react during feed preparation and drying. For example,  $\text{Al}(\text{NO}_3)_3 \cdot 9\text{H}_2\text{O}$  dehydrates and reacts with NaOH.
- At  $200^\circ\text{C}$ , sucrose melts.
- At  $300^\circ\text{C}$ , all organics and alkali salts form eutectic melt. Carbonates have high individual melting points, and thus do not readily dissolve in the small fraction of eutectic salt mixture that forms during HLW feed heating. However, we assume that they dissolve during LAW feed melting when a significant volume of nitrate/nitrite salt melt evolves.
- At higher temperatures, the fraction of molten salts decreases as its components continue to react and decompose—their disappearance was estimated using gas evolution data from EGA.

## 5.2 | Molten salt migration

While the fraction of low-viscosity molten salt in the HLW feed is low (below 5 mass %), Figure 6 indicates that the fraction of molten salt in the LAW feed can reach up to 28 mass %, possibly exceeding  $v_C$ , the critical volume fraction for the onset of molten salt migration, reported in Hirma et al.<sup>35</sup> and Kim et al.<sup>37</sup> This can result in the segregation of molten salt from the refractory particles during melting, leading to interruptions in the steady-state melting process and reduced production rates. Molten salt migra-

tion has been observed in various contexts, such as in cold cap samples retrieved from a research-scale melter,<sup>44</sup> where an alkali-enriched salt layer was detected above the primary foam layer; during the design of the bulk vitrification process<sup>45</sup>; or in fast-dried slurry samples prepared in laboratory to resemble LAW and HLW cold cap structure.<sup>7,41</sup>

Fortunately, the molten salt drainage is not problematic as it is typically halted in lower parts of the cold cap where connected melt creates a barrier for further downward migration. This leads to the formation of an alkali-enriched layer, which can facilitate the reaction between molten salt and refractory particle at an accelerated rate because of higher temperatures in the lower parts of the cold cap. However, as mentioned in Section 2, the horizontal migration of excess molten salt can impoverish refractory components of fluxes and could potentially lead to a frozen cold cap.<sup>35</sup>

## 5.3 | Molten salt and Re retention

Another important phenomenon that is significantly affected by the presence of molten salt and its coexistence with glass-forming melt is the retention of radioactive technetium and its nonradioactive surrogate, rhenium. Recent studies<sup>15,43,46,47</sup> suggested that the Tc/Re retention is determined by the differences in the Tc/Re diffusion from the molten salt phase (consisting of carbonates, nitrates, nitrites, sulfates, and chromates), where Tc/Re is initially present,<sup>47</sup> into the transient glass-forming (mostly alkali-alumino-silico-borate) melt. After nitrates, nitrites, and carbonates decompose between  $200\text{--}700^\circ\text{C}$ , the perrhenate/pertechnetate-containing sulfate-chromate-perrhenate phase that remains undissolved in the glass-forming melt<sup>43,47</sup> may segregate on the melt surface, where Re rapidly volatilizes.<sup>48</sup>

We have recently suggested that various glass-forming and -modifying additives may affect the Tc/Re retention by enhancing the Tc/Re diffusion from the molten salt phase into the nascent glass-forming melt.<sup>15,49</sup> Specifically, we showed that the addition of reducing agents such as sucrose increased Tc/Re retention while not affecting Tc/Re speciation. By reacting with nitrates and nitrites at low temperatures, a higher sucrose content decreases the fraction of the molten salt phase in the temperature range between  $400\text{--}700^\circ\text{C}$ , increasing the driving force for the rhenium diffusion from the molten salt phase into the glass-forming melt, both by creating higher a concentration difference and a larger contact surface between these two media.

In addition, we previously reported that the Re retention in AP-107 LAW glass was lower than in a compositionally

**TABLE 3** Re retention in series of AN-102 low-activity waste (LAW) feeds with different sources of alumina (standard deviation is based on duplicate measurement).

| Alumina source in the feed  | Re retention (%) |
|---|------------------|
| Al <sub>2</sub> SiO <sub>5</sub> (nominal)                          | 48 ± 2           |
| Al <sub>2</sub> SiO <sub>5</sub> /Al(OH) <sub>3</sub> (50/50 wt. %) | 58 ± 1           |
| Al(OH) <sub>3</sub>   | 67 ± 0           |

similar AN-105 LAW glass<sup>15</sup>; the alumina source in AP-107 LAW melter feed was kyanite, Al<sub>2</sub>SiO<sub>5</sub>, whereas AN-105 LAW feed contained mostly gibbsite, Al(OH)<sub>3</sub>, with a low fraction of kyanite. Xu et al.<sup>50</sup> attributed the higher Re retention to the adsorption of residual sulfate-perrhenate melt on amorphous alumina of a high specific surface area that was produced from Al(OH)<sub>3</sub> on heating. To test this hypothesis, we prepared AN-102 LAW melter feeds (compositionally similar to the AP-107 LAW,<sup>47</sup> see Supplementary material, Supplementary Table S1) with kyanite, 50 % kyanite substituted with gibbsite, and kyanite fully replaced with gibbsite. The feeds were spiked with Re<sub>2</sub>O<sub>7</sub> solution corresponding to 300 ppm Re in glass. Approximately 50 g of dry powder feed was heated in glazed porcelain crucibles at 10 K min<sup>-1</sup> under an air atmosphere from room temperature to 1150°C. After quenching, the samples were ground and crushed to below 100 μm grain size, and the Re content was analyzed by inductively coupled plasma mass spectrometry. As Table 3 shows, replacing kyanite with gibbsite enhanced sulfate-perrhenate dissolution in the glass-forming melt, and reduced the rate of sulfate-perrhenate segregation and volatilization.

Further analysis of the effect of alumina and other GFMA's on the Re diffusion from the molten salt phase into the glass-forming melt and the resulting Re retention in the produced glass will be reported in a follow-up study,<sup>51</sup> in which we will also report that when NaSiO<sub>3</sub> or NaOH is used in the feed instead of NaNO<sub>3</sub>, the Re retention can reach almost 100%—also suggesting that if molten salt formation is significantly reduced or even prevented (with boric acid, both NaSiO<sub>3</sub> or NaOH create a sodium-borate gel that, on heating, turns into the glass-forming melt), Re can be fully incorporated into the glass-forming melt and its volatilization diminished.

## 5.4 | Transient glass-forming melt and primary foaming

Figure 8 displays optical microscopy images of HLW feed samples quenched in the air after heating to temperatures 700, 800, 900, and 1000°C. The glass-forming melt, once connected, encapsulates dissolving refractory particles and irregularly shaped pores (Figure 8A) that soon

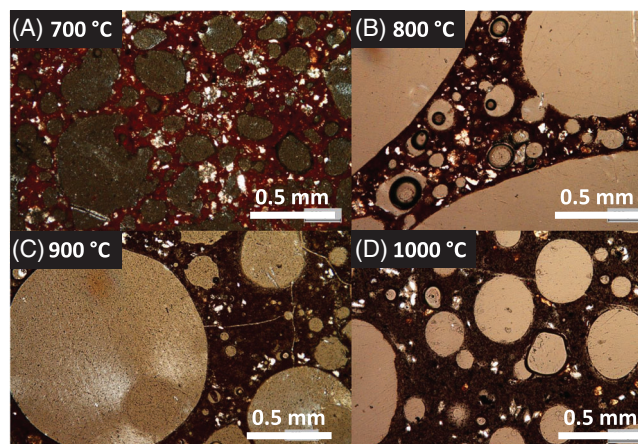


**FIGURE 8** Optical microscopy image of the high-level waste (HLW) sample heated to (A) 700, (B) 800, (C) 900, and (D) 1000°C. Gas bubbles are separated by glass-forming melt, in which residual refractory particles are dissolving (visible as bright spots in the polarized image).

become spherical as temperature increases, thus turning the melt into primary foam.<sup>52</sup> As temperature increases, the primary foam porosity grows due to residual gas evolution and thermal expansion. At the temperature of the maximum foam volume,  $T_{FM} = \sim 800^\circ\text{C}$  (Figure 8B), the foam porosity reaches  $\sim 75\%$  (c.f., Figure 4), and the foam structure consists of larger bubbles, separated by lamellae filled with smaller bubbles. The foam is eventually destabilized and starts to internally collapse, caused partly by the increasing porosity, partly by decreasing transient melt viscosity, and, in the cold cap, also by the shear stress imposed by the melt flow below the cold cap (Figure 8C,D).

Primary foam structure has been observed using both in situ and ex situ X-ray tomography<sup>25,26,29,53–55</sup> and in quenched cold caps produced using laboratory-scale melters.<sup>56</sup> While the foam structure changes during quenching due to the thermal contraction of gas that continues until viscosity drops below  $\sim 10^6$  Pa s, the in situ X-ray tomography captures the primary foam structure at high temperatures. Using different experimental setups, both Luksic et al.<sup>25</sup> and Harris et al.<sup>54</sup> were able to reliably discern bubbles with a diameter  $> \sim 0.8$  mm.

The gas bubbles in the primary foam are separated by lamellae consisting of glass-forming melt in which residual refractory particles continue to dissolve, mainly silica, kyanite, zircon, and spinels. The properties of this condensed phase, especially its viscosity, determine the foam behavior: its onset temperature, collapse temperature, and maximum porosity. In a previous study using different HLW and LAW melter feeds, we found that<sup>28,31</sup>: (i) the fraction of the glass-forming melt to encapsulate the bubbles depends on glass-forming melt viscosity—it increased by 10% for each order of magnitude increase in the

glass-forming melt viscosity, and (ii) the foam collapse might occur in a relatively narrow range of glass-forming melt viscosity—between 20 and 90 Pa s, and (iii) the fraction of undissolved silica affects the primary foam stability.

## 6 | SUMMARY AND FUTURE PERSPECTIVES

Despite decades of research, numerous opportunities still exist to enhance the waste vitrification process, increase its rate, and reduce its cost. Because of unanswered questions in the kinetics and thermodynamics of glass batch melting,<sup>57,58</sup> these opportunities have often not been fully explored or realized. In this study, we aimed to shed light on a fundamental aspect of this process—the evolution of molten salt and transient glass-forming melt—and to elucidate several phenomena related to it. Here, we would like to outline possible directions for further research.

### 6.1 | Primary foaming

Primary foaming is a phenomenon not unique to nuclear waste glass melting but is a concern for commercial glass melting as well. Regrettably, despite its strong effect on the heat transfer into the batch and on the final glass quality, primary foaming remains one of the least understood phenomena during glass melting. Following our earlier studies showcasing the importance of primary foam behavior for the evaluation of heat transfer to the batch,<sup>5</sup> a number of studies followed, focusing on the primary foam structure and the kinetics of foaming. This included (i) high-temperature visual observation and later also in-situ X-ray tomography evaluating the foam porosity, bubble size distribution, and the mechanism of foam coalescence and collapse,<sup>25,55</sup> and (ii) kinetic studies analyzing how the temperature interval of primary foaming and the foam structure depend on the batch thermal history.<sup>59</sup>

These techniques allow us to observe and investigate the primary foam behavior in a broad range of commercial and waste glass batches, have been used to develop kinetic models for their conversion,<sup>27</sup> and were implemented in the computational dynamics model of glass melters.<sup>8,60</sup> Although the effects of batch formulation and pre-treatment on the extent of primary foaming were analyzed in the past,<sup>61–63</sup> their fundamental understanding is still lacking. The three main questions are: How do the properties of the transient glass-forming melt, such as viscosity, surface tension, or density, change during the conversion process? How do these properties, the transient glass-forming melt fraction, and the gas-evolving

reactions affect the primary foam extent, behavior, and stability? And how can the transition from a trial-and-error paradigm toward a model-based design of glass batch formulation exhibiting limited primary foaming be accomplished?

### 6.2 | Technetium/Rhenium retention

During the vitrification of nuclear waste, one of the main radionuclides of concern is Tc-99. Next to the concerns caused by long half-life and high mobility in the environment,<sup>64</sup> Tc is also highly volatile, resulting in its low retention in the waste glass.<sup>65–67</sup> Although the volatilized Tc is commonly captured in the off-gas treatment system and typically recycled back to the melter to increase its retention (and avoid costs with a separate Tc immobilization into other waste forms), this causes other problems—other volatile components of the recycle stream (such as sulfur and chlorine) decrease the loading of waste in the glass,<sup>68</sup> increasing the glass volume. Thus, a significant amount of work has been performed in the past both on the immobilization of Tc and its nonradioactive surrogate, Re, whose volatility generally exhibits behavior analogous to that of Tc, regardless of the differences in their ionic size or speciation in glass.<sup>69,70</sup>

Initially, Tc/Re is a component in the molten salt phase (consisting of carbonates, nitrates, nitrites, sulfates, and chromates).<sup>47</sup> During melting, nitrates, nitrites, and carbonates decompose, releasing gases and forming nascent glass-forming borate and borosilicate melts, while at the same time, Tc/Re diffuses from the molten salt phase into the glass-forming melt. The fraction of Tc/Re that is not incorporated in the glass-forming melt by 800°C then forms a segregated salt phase from which Tc/Re fully volatilizes by 1100°C.

The Tc/Re incorporation into the glass structure is not limited by the Tc and Re solubility, which is ~1500–3000 ppm,<sup>70–72</sup> more than two orders of magnitude higher than the Tc/Re concentration targets in the produced nuclear waste glass, <10 ppm.<sup>73</sup> Thus, it is the rate of diffusion from the molten salt into the glass-forming phase that affects the retention of Tc/Re. As described in Section 5.3, Tc/Re diffuses into the nascent glass-forming melt, initially from the molten salt phase<sup>47</sup> consisting of the full range of oxyanionic components, and eventually from the remaining sulfate-chromate melt that tends to segregate and release Tc/Re into the atmosphere. The main questions thus are—what are the controlling factors for the diffusion of Tc/Re from the salt phase into the glass-forming melt, and how to accomplish the full retention of Tc/Re from the salt phase into the glass product?

### 6.3 | Segregation of molten salts, yellow phase formation

Melting instability caused by demixing phenomena within the cold cap is one of the several problems that can be potentially encountered both during the melting of commercial glass batches and during the vitrification of nuclear waste. Several demixing phenomena have been reported, including (i) evaporation of volatile components, (ii) drainage of low-viscosity melts, (iii) segregation of melts with different densities, and (iv) settling or buoyancy of solid particles. Because most of the glass melt surface is not exposed to the furnace atmosphere, the evaporation of volatile components is significantly reduced during all-electric melting with a cold cap. Moreover, feed components that volatilize during the feed-to-glass conversion can condense in cooler sections—this reflux phenomenon is well-known in industrial batch blankets.<sup>74</sup>

However, the segregation of low-viscosity molten salt can cause troublesome problems. Potentially prone to molten salt segregation via migration are LAW feeds that contain large fractions of alkali nitrates, nitrites, and carbonates.<sup>35,37</sup> The warning signs of its occurrence and methods of its prevention are open questions to be addressed before it occurs during the large-scale operation.

The residual low-density salt phase consisting of sulfates, chromates, and molybdates tends to segregate from the glass melt, forming the so-called “yellow phase”, the formation of which limits the waste loading in the glass. Yellow phase has been a topic of research around the world, including the US,<sup>75–78</sup> France,<sup>79,80</sup> Japan,<sup>81,82</sup> the UK,<sup>83,84</sup> and also China,<sup>85–88</sup> where first waste vitrification facilities have recently been constructed and will need to immobilize nuclear waste containing significant concentrations of sulfate. Significant advancements have been achieved, for example showing that the salt segregation can be suppressed by the redistribution of oxides from the original glass frit to the waste simulant, by glass composition reformulation, or by milling the frit into powder, but, as a recent review noted, an industrial solution has not yet been implemented.<sup>18</sup> The question still remains—how to optimize both batch and glass compositions in order to maximize the incorporation of low-miscible salts into the glass-forming melt?

## 7 | CONCLUSIONS

In this work, we used high-temperature environmental scanning electron microscopy, X-ray diffraction, evolved gas analysis, and thermogravimetry to analyze the reaction pathways and phase transitions during the melt-

ing of nuclear waste melter feeds. After estimating the compositions of amorphous phases and fractions of salt components in the feed, we specifically focused on the issue of primary melt (molten salt) formation. We showed that significant amounts of molten salt can be present during the melting of low-activity waste feeds. This can potentially lead to unwanted demixing phenomena in the cold cap, such as the segregation of molten salts from refractories in the early stages of melting or formation of secondary liquid phases in the later stages, and significantly affect other process parameters, such as retention of Tc/Re.

The key open questions related to the molten salt phase and glass-forming melt formation are: (i) What are the criteria for the onset of molten salt migration in the early stages of melting? (ii) What are the criteria for the formation of a secondary salt phase at higher temperatures, and how to optimize the feed and glass composition to prevent its formation? (iii) What are the controlling factors for the diffusion of Tc/Re from the molten salt phase into the transient glass-forming melt, and how to accomplish full retention of Tc/Re in the glass? and (iv) How do the fraction and properties of both the molten salt phase and the transient glass-forming phase affect the feed primary foaming? Answering these questions will help achieve stable and high melting rates during the vitrification of high waste-loading melter feeds.

### ACKNOWLEDGMENTS

Richard Pokorný, Miroslava Vernerová, Jaroslav Kloužek, Petra Cincibusová, and Radek Pezl gratefully acknowledge financial support from the Czech Ministry of Education, Youth and Sports, project number: LUAUS23062. The authors gratefully acknowledge the financial support provided by the U.S. Department of Energy (DOE) Waste Treatment and Immobilization Plant Project. Pacific Northwest National Laboratory is operated by Battelle for DOE under contract DE-AC05-76RL01830.

### ORCID

Richard Pokorný  <https://orcid.org/0000-0002-9023-0381>

Petra Cincibusová  <https://orcid.org/0000-0002-2164-3713>

Pavel Ferkl  <https://orcid.org/0000-0003-2844-3199>

Renaud Podor  <https://orcid.org/0000-0002-8103-1743>

### REFERENCES

1. Gray RH, Becker CD. Environmental cleanup: the challenge at the Hanford Site, Washington, USA. *Environ Manage.* 1993;17(4):461–75.

2. Crowley KD, Ahearne JF. Managing the environmental legacy of U.S. nuclear-weapons production: although the waste from America's arms buildup will never be "cleaned up," human and environmental risks can be reduced and managed. *Am Sci*. 2002;90(6):514–23.
3. Vienna JD. Nuclear waste vitrification in the United States: recent developments and future options. *Int J Appl Glass Sci*. 2010;1(3):309–21.
4. Goel A, Mccloy JS, Pokorny R, Kruger AA. Challenges with vitrification of hanford high-level waste (HLW) to borosilicate glass—an overview. *Journal of Non-Crystalline Solids: X*. 2019;4:100033.
5. Pokorny R, Hilliard ZJ, Dixon DR, Schweiger MJ, Guillen DP, Kruger AA, et al. One-dimensional cold cap model for melters with bubblers. *J Am Ceram Soc*. 2015;98(10):3112–8.
6. Lu X, Kim D-S, Vienna JD. Impacts of constraints and uncertainties on projected amount of Hanford low-activity waste glasses. *Nucl Eng Des*. 2021;385:111543.
7. Hujová M, Klouzek J, Cutforth DA, Lee S, Miller MD, Mccarthy B, et al. Cold-cap formation from a slurry feed during nuclear waste vitrification. *Ceram Int*. 2019;45(5):6405–12.
8. Pokorný R, Hrma P, Lee S, Klouzek J, Choudhary MK, Kruger AA. Modeling batch melting: Roles of heat transfer and reaction kinetics. *J Am Ceram Soc*. 2020;103(2):701–18.
9. Pokorný R, Pierce DA, Hrma P. Melting of glass batch: model for multiple overlapping gas-evolving reactions. *Thermochim Acta*. 2012;541:8–14.
10. Pokorny R, Rice JA, Crum JV, Schweiger MJ, Hrma P. Kinetic model for quartz and spinel dissolution during melting of high-level-waste glass batch. *J Nucl Mater*. 2013;443(1):230–5.
11. Henager SH, Hrma P, Swearingen KJ, Schweiger MJ, Marcial J, Tegrotenhuis NE. Conversion of batch to molten glass, I: volume expansion. *J Non-Cryst Solids*. 2011;357(3):829–35.
12. Hrma P, Marcial J, Swearingen KJ, Henager SH, Schweiger MJ, Tegrotenhuis NE. Conversion of batch to molten glass, II: dissolution of quartz particles. *J Non-Cryst Solids*. 2011;357(3):820–8.
13. Lee S, Cutforth DA, Mar D, Klouzek J, Ferkl P, Dixon DR, et al. Melting rate correlation with batch properties and melter operating conditions during conversion of nuclear waste melter feeds to glasses. *Int J Appl Glass Sci*. 2021;12(3):398–414.
14. Ferkl P, Hrma P, Klouzek J, Vernerová M, Kruger A, Pokorný R. Model for batch-to-glass conversion: coupling the heat transfer with conversion kinetics. *Journal of Asian Ceramic Societies*. 2021;9(2):652–64.
15. Khawand J, Klouzek J, Vernerová M, Cincibusová P, Hrma P, Kruger AA, et al. Effect of sucrose on the oxidation-reduction conditions and retention of rhenium during vitrification of low-activity waste. *J Nucl Mater*. 2023;573:154155.
16. Muller IS, Mckeown DA, Pegg IL. Structural Behavior of Tc and I ions in nuclear waste glass. *Procedia Materials Science*. 2014;7:53–9.
17. Sargin I, Lonergan CE, Vienna JD, Mccloy JS, Beckman SP. A data-driven approach for predicting nepheline crystallization in high-level waste glasses. *J Am Ceram Soc*. 2020;103(9):4913–24.
18. Mccloy JS, Schuller S. Vitrification of wastes: from unwanted to controlled crystallization, a review. *Comptes Rendus. Géoscience*. 2022;354(S1):121–60.
19. Walling SA, Kauffmann MN, Gardner LJ, Bailey DJ, Stennett MC, Corkhill CL, et al. Characterisation and disposability assessment of multi-waste stream in-container vitrified products for higher activity radioactive waste. *J Hazard Mater*. 2021;401:123764.
20. Bingham PA, Hyatt NC, Hand RJ. Vitrification of UK intermediate level radioactive wastes arising from site decommissioning: property modelling and selection of candidate host glass compositions. *Glass Technology—European Journal of Glass Science and Technology Part A*. 2012;53(3):83–100.
21. Tan S, Kirk N, Marshall M, Mcgann O, Hand RJ. Vitrification of an intermediate level Magnox sludge waste. *J Nucl Mater*. 2019;515:392–400.
22. Xu K, Hrma P, Rice J, Riley BJ, Schweiger MJ, Crum JV. Melter feed reactions at  $T \leq 700^\circ\text{C}$  for nuclear waste vitrification. *J Am Ceram Soc*. 2015;98(10):3105–11.
23. Xu K, Hrma P, Rice JA, Schweiger MJ, Riley BJ, Overman NR, et al. Conversion of nuclear waste to molten glass: cold-cap reactions in crucible tests. *J Am Ceram Soc*. 2016;99(9):2964–70.
24. Hujova M, Pokorny R, Klouzek J, Lee S, Traverso JJ, Schweiger MJ, et al. Foaming during nuclear waste melter feeds conversion to glass: application of evolved gas analysis. *Int J Appl Glass Sci*. 2018;9:487–98.
25. Luksic SA, Pokorny R, George J, Hrma P, Varga T, Reno LR, et al. In situ characterization of foam morphology during melting of simulated waste glass using x-ray computed tomography. *Ceram Int*. 2020;46(11 Part A):17176–85.
26. Luksic SA, Pokorny R, Hrma P, Varga T, Rivers EL, Buchko AC, et al. Through a glass darkly: In-situ x-ray computed tomography imaging of feed melting in continuously fed laboratory-scale glass melter. *Ceram Int*. 2021;47(11):15807–18.
27. Ueda N, Vernerová M, Klouzek J, Ferkl P, Hrma P, Yano T, et al. Conversion kinetics of container glass batch melting. *J Am Ceram Soc*. 2021;104(1):34–44.
28. Ferkl P, Hrma P, Abboud A, Guillen DP, Khawand J, Kopal I, et al. Conversion kinetics during melting of simulated nuclear waste glass feeds measured by dissolution of silica. *J Non-Cryst Solids*. 2022;579:121363.
29. Marcial J, Luksic S, Klouzek J, Vernerová M, Cutforth D, Varga T, et al. In-situ X-ray and visual observation of foam morphology and behavior at the batch-melt interface during melting of simulated waste glass. *Ceram Int*. 2022;48(6):7975–85.
30. Rigby JC, Dixon DR, Cutforth DA, Marcial J, Klouzek J, Pokorný R, et al. Melting behaviour of simulated radioactive waste as functions of different redox iron-bearing raw materials. *J Nucl Mater*. 2022;569:153946.
31. Lee SM, Mccarthy BP, Hrma P, Chun J, Pokorny R, Klouzek J, et al. Viscosity of glass-forming melt at the bottom of high-level waste melter-feed cold caps: effects of temperature and incorporation of solid components. *J Am Ceram Soc*. 2020;103(3):1615–30.
32. Podor R, Pailhon D, Ravaux J, Brau H-P. Development of an integrated thermocouple for the accurate sample temperature measurement during high temperature environmental scanning electron microscopy (HT-ESEM) experiments. *Microsc Microanal*. 2015;21(2):307–12.
33. Podor R, Bouala GIN, Ravaux J, Lautru J, Clavier N. Working with the ESEM at high temperature. *Mater Charact*. 2019;151:15–26.

34. Podor R, Schuller S, Ravauxa J, Monteiro A, Boucetta H, Delattre O, et al. In Situ ESEM experiment applied to the description of chemical processes during glass elaboration. *Procedia Materials Science*. 2014;7:111–6.
35. Hrma P, Gales CE, Yasuda DD. Drainage of primary melt in a glass batch. *Ceramic Transactions*. 1991;23:361–7.
36. Hrma P, Klouzek J, Pokorny R, Lee SM, Kruger AA. Heat transfer from glass melt to cold cap: Gas evolution and foaming. *J Am Ceram Soc*. 2019;102(10):5853–65.
37. Kim D-S, Bagaasen LM, Crum JV, Fluegel A, Gallegos A, Martinez B, et al. Investigation of Tc migration mechanism during bulk vitrification process using re surrogate. Richland, WA: PNNL; 2006.
38. Kruger AA, Pegg IL, Chaudhuri M, Gong W, Gan H, Matlack KS, et al. Melt rate enhancement for high aluminum HLW glass formulations. Richland, WA: Office of River Protection; 2008.
39. Matlack KS, Abramowitz H, Muller IS, Joseph I, Pegg IL. DFLAW Glass and Feed Qualifications for AP-107 to Support WTP Start-Up and Flow-Sheet Development, VSL-18R4500-1: United States. 2018.
40. Schweiger MJ, Hrma P, Humrickhouse CJ, Marcial J, Riley BJ, Tegrotenhuis NE. Cluster formation of silica particles in glass batches during melting. *J Non-Cryst Solids*. 2010;356(25):1359–67.
41. Hujova M, Klouzek J, Cutforth D, Lee S, Miller M, Kruger A, et al. Feed-to-glass conversion during low activity waste vitrification. *Ceram Int*. 2020;46(7):9826–33.
42. Appel CJ, Klouzek J, Jani N, Lee SM, Dixon DR, Hrma P, et al. Effect of sucrose on foaming and melting behavior of a low-activity waste melter feed. *J Am Ceram Soc*. 2019;102(12):7594–605.
43. Jin T, Kim D, Kruger AA. Effects of sulfate on rhenium incorporation into low-activity waste glass. *J Non-Cryst Solids*. 2019;521:119528.
44. Whittington KF, Seiler DK, Luey J, Vienna JD, Sliger WA. Feed process studies—research-scale melter. Richland, WA: PNNL; 1996.
45. Hrma PR, Bagaasen LM, Schweiger MJ, Evans MB, Smith BT, Arrigoni BM, et al. Bulk vitrification performance enhancement: refractory lining protection against molten salt penetration. Richland, WA: PNNL; 2007.
46. Jin T, Kim D, Tucker AE, Schweiger MJ, Kruger AA. Reactions during melting of low-activity waste glasses and their effects on the retention of rhenium as a surrogate for technetium-99. *J Non-Cryst Solids*. 2015;425:28–45.
47. George JL, Kim D, Kruger AA. Effects of iron oxalate on rhenium incorporation into low-activity waste glass. *J Non-Cryst Solids*. 2020;545:120257.
48. Hrma P, Vienna JD, Wilson BK, Plaisted TJ, Heald SM. Chromium phase behavior in a multi-component borosilicate glass melt. *J Non-Cryst Solids*. 2006;352(21):2114–22.
49. Lee S, Jin T, Rivers E, Klouzek J, Luksic S, Marcial J, et al. Effect of sucrose on technetium and rhenium retention during vitrification of low-activity wastes. *J Am Ceram Soc*. 2022;105(12):7321–33.
50. Xu K, Hrma P, Washton N, Schweiger MJ, Kruger AA. Conversion of nuclear waste to molten glass: formation of porous amorphous alumina in a high-Al melter feed. *J Nucl Mater*. 2017;483:102–6.
51. Vernerová M. Effect of alumina source and oxyanionic salts on the Re retention during vitrification of nuclear waste. In preparation, 2023.
52. Dixon DR, Schweiger MJ, Riley BJ, Pokorny R, Hrma P. Temperature distribution within a cold cap during nuclear waste vitrification. *Environ Sci Technol*. 2015;49(14):8856–63.
53. Watanabe K, Yano T, Takeshita K, Minami K, Ochi E. X-ray CT imaging of vitrified glasses containing simulant radioactive wastes: Structure and chemical reactions of glass beads and wastes in the cold cap. *Glass Technology—European Journal of Glass Science and Technology Part A*. 2012;53(6):273–8.
54. Harris WH, Guillen DP, Klouzek J, Pokorny R, Yano T, Lee S, et al. X-ray tomography of feed-to-glass transition of simulated borosilicate waste glasses. *J Am Ceram Soc*. 2017;100(9):3883–94.
55. Boloré D, Gibilaro M, Massot L, Chamelot P, Cid E, Masbernat O, et al. X-ray imaging of a high-temperature furnace applied to glass melting. *J Am Ceram Soc*. 2020;103(2):979–92.
56. Lee S, Hrma P, Pokorny R, Klouzek J, Vanderveer BJ, Dixon DR, et al. Effect of melter feed foaming on heat flux to the cold cap. *J Nucl Mater*. 2017;496:54–65.
57. Mauro JC, Philip CS, Vaughn DJ, Pambianchi MS. Glass Science in the United States: current status and future directions. *Int J Appl Glass Sci*. 2014;5(1):2–15.
58. Mauro JC, Zanolto ED. Two centuries of glass research: Historical trends, current status, and grand challenges for the future. *Int J Appl Glass Sci*. 2014;5(3):313–27.
59. Lee SM, Hrma P, Pokorny R, Traverso JJ, Klouzek J, Schweiger MJ, et al. Heat transfer from glass melt to cold cap: effect of heating rate. *Int J Appl Glass Sci*. 2019;10(3):401–13.
60. Abboud AW, Guillen DP, Hrma P, Kruger AA, Klouzek J, Pokorny R. Heat transfer from glass melt to cold cap: computational fluid dynamics study of cavities beneath cold cap. *Int J Appl Glass Sci*. 2021;12(2):233–44.
61. Lee S, Vanderveer BJ, Hrma P, Hilliard ZJ, Heilman-Moore JS, Bonham CC, et al. Effects of heating rate, quartz particle size, viscosity, and form of glass additives on high-level waste melter feed volume expansion. *J Am Ceram Soc*. 2017;100(2):583–91.
62. Lee S, Hrma P, Pokorny R, Klouzek J, Vander Veer BJ, Rodriguez CP, et al. Effects of alumina sources (gibbsite, boehmite, and corundum) on melting behavior of high-level radioactive waste melter feed. *MRS Advances*. 2017;2(11):603–8.
63. Doi Y, Yano T, McCarthy BP, Schweiger MJ, Hrma P. Effects of particle size and briquetting of soda-lime-silicate glass batch on viscosity during batch-to-melt conversion. *Int J Appl Glass Sci*. 2019;10(1):115–24.
64. Lukens WW, Mckeown DA, Buechele AC, Muller IS, Shuh DK, Pegg IL. Dissimilar behavior of technetium and rhenium in borosilicate waste glass as determined by X-ray absorption spectroscopy. *Chem Mater*. 2007;19(3):559–66.
65. Pegg IL. Behavior of technetium in nuclear waste vitrification processes. *J Radioanal Nucl Chem*. 2015;305(1):287–92.
66. Dixon DR, Hall MA, Lang JB, Cutforth DA, Stewart CM, Eaton WC. Retention analysis from vitrified low-activity waste and simulants in a laboratory-scale melter. *Ceram Int*. 2022;48(5):5955–64.
67. Niu C, Zhao C, Zhou X, Xu K. Immobilization of Technetium-99 in a lead borosilicate glass. *J Non-Cryst Solids*. 2023;603:122110.

68. Vienna JD, Kim DS, Skorski DC, Matyas J. Glass property models and constraints for estimating the glass to be produced at Hanford by implementing current advanced glass formulation efforts. US Department of Energy; 2013. <https://doi.org/10.2172/1170502>
69. Xu K, Pierce DA, Hrma P, Schweiger MJ, Kruger AA. Rhenium volatilization in waste glasses. *J Nucl Mater.* 2015;464:382–8.
70. McCloy JS, Riley BJ, Goel A, Liezers M, Schweiger MJ, Rodriguez CP, et al. Rhenium solubility in borosilicate nuclear waste glass: Implications for the processing and immobilization of technetium-99. *Environ Sci Technol.* 2012;46(22):12616–22.
71. Gan H, Mckeown DA, Xie X, Pegg IL. Assessment of rhenium as a surrogate for technetium in Hanford low activity waste borosilicate glasses: speciation, solubility, and redox effects. *Int J Appl Glass Sci.* 2023;14(1):97–112.
72. Midorikawa M, Gan H, Mckeown DA, Xie X, Yano T, Pegg IL. Speciation and solubility of rhenium in borosilicate waste glasses. *J Non-Cryst Solids.* 2022;580:121219.
73. Kim D-S, Vienna J, Hrma P, Schweiger MJ, Matyas J, Crum JV, et al. Development and testing of ICV glasses for Hanford LAW. Richland, WA: PNNL; 2003.
74. Davis RE. Batch blanket chemistry and air quality emissions associated with cold-top electric furnaces. In: *Proceedings of the 46th Conference on Glass Problems: Ceramic Engineering and Science Proceedings.* OH, US: The American Ceramic Society, Inc ;1986. p. 460–6.
75. Brehault A, Patil D, Kamat H, Youngman RE, Thirion LM, Mauro JC, et al. Compositional dependence of solubility/retention of molybdenum oxides in aluminoborosilicate-based model nuclear waste glasses. *J Phys Chem B.* 2018;122(5):1714–29.
76. Patil DS, Konale M, Gabel M, Neill OK, Crum JV, Goel A, et al. Impact of rare earth ion size on the phase evolution of MoO<sub>3</sub>-containing aluminoborosilicate glass-ceramics. *J Nucl Mater.* 2018;510:539–50.
77. Saini R, Kapoor S, Neuville DR, Youngman RE, Cerrutti BM, McCloy JS, et al. Correlating sulfur solubility with short-to-intermediate range ordering in the structure of borosilicate glasses. *J Phys Chem C.* 2022;126(1):655–74.
78. Xu X, Youngman RE, Kapoor S, Goel A. Structural drivers controlling sulfur solubility in alkali aluminoborosilicate glasses. *J Am Ceram Soc.* 2021;104(10):5030–49.
79. Boué E, Schuller S, Toplis MJ, Charpentier T, Mesbah A, Pablo H, et al. Kinetic and thermodynamic factors controlling the dissolution of molybdate-bearing calcines during nuclear glass synthesis. *J Nucl Mater.* 2019;519:74–87.
80. Schuller S, Benigni P, Gossé S, Bégaud-Bordier S, Mikaelian G, Podor R, et al. Liquid-liquid phase separation in borosilicate glass enriched in MoO<sub>3</sub> – experimental investigations and thermodynamic calculations. *J Non-Cryst Solids.* 2023;600:121997.
81. Uruga K, Tsukada T, Usami T. Generation mechanism and prevention method of secondary molybdate phase during vitrification of PUREX wastes in liquid-fed ceramic melter. *J Nucl Sci Technol.* 2020;57(4):433–43.
82. Gan H, Matlack KS, Pegg IL, Joseph I, Bowan BW, Miura Y, et al. Suppression of yellow phase formation during Japanese HLW vitrification. In *ceramics for environmental and energy applications II.* (eds Dogan F, Tritt TM, Sekino T, Katoh Y, Pyzik AJ, Belharouak I, Boccaccini AR, Marra J, and Lin HT). 2014, p. 237–50. <https://doi.org/10.1002/9781118771327.ch23>
83. Short R. Phase separation and crystallisation in UK HLW vitrified products. *Procedia Materials Science.* 2014;7:93–100.
84. Bingham PA, Vaishnav S, Forder SD, Scrimshire A, Jaganathan B, Rohini J, et al. Modelling the sulfate capacity of simulated radioactive waste borosilicate glasses. *J Alloys Compd.* 2017;695:656–67.
85. Lei J, Wang B, Xu L, Teng Y, Li Y, Deng H, et al. Role of Ba(NO<sub>3</sub>) pretreatment in reducing the yellow phase formation during vitrification of nuclear waste. *J Nucl Mater.* 2021;555:153121.
86. Wang XQ, Tuo XG, Zhou H, Zhang W, Li Z, Chen XL, et al. Glass formulation development on high-sodium and high-sulfur bearing high level liquid waste for vitrification process. *He-Huaxue yu Fangshe Huaxue/Journal of Nuclear and Radiochemistry.* 2013;35(3):180–92.
87. Lian Q, Zhang Z, Wang B, Yao Y, Zhao X, Wu L. Effects of Ba(NO<sub>3</sub>)<sub>2</sub> content on yellow phase formation and chemical durability of vitrified waste glass. *J Non-Cryst Solids.* 2022;597:121933.
88. Wu L, Xiao J, Wang X, Teng Y, Li Y, Liao Q. Crystalline phase, microstructure, and aqueous stability of zirconolite-barium borosilicate glass-ceramics for immobilization of simulated sulfate bearing high-level liquid waste. *J Nucl Mater.* 2018;498:241–8.

## SUPPORTING INFORMATION

Additional supporting information can be found online in the Supporting Information section at the end of this article.

**How to cite this article:** Pokorný R, Vernerová M, Kloužek J, Cincibusová P, Kohoutková M, Pezl R, et al. Transient melt formation and its effect on conversion phenomena during nuclear waste vitrification – HT-ESEM analysis. *J Am Ceram Soc.* 2024;107:1691–1705.  
<https://doi.org/10.1111/jace.19361>